Schwann Cell Myelination Requires Timely and Precise Targeting of P_0 Protein

X. Yin,* G.J. Kidd,* L. Wrabetz,‡ M.L. Feltri,‡ A. Messing,§ and B.D. Trapp*

*Department of Neurosciences, Lerner Research Institute, Cleveland Clinic Foundation, Cleveland, Ohio 44195; ‡Department of Neurology and Department of Biological and Technological Research (DIBIT), San Raffaele Scientific Institute, 20132 Milano, Italy; and §Waisman Center and Department of Pathobiological Sciences, School of Veterinary Medicine, University of Madison-Wisconsin, Madison, Wisconsin 53705

Abstract. This report investigated mechanisms responsible for failed Schwann cell myelination in mice that overexpress P_0 (P_0^{tg}), the major structural protein of PNS myelin. Quantitative ultrastructural immunocytochemistry established that P_0 protein was mistargeted to abaxonal, periaxonal, and mesaxon membranes in P_0^{tg} Schwann cells with arrested myelination. The extracellular leaflets of P_0-containing mesaxon membranes were closely apposed with periodicities of compact myelin. The myelin-associated glycoprotein was appropriately sorted in the Golgi apparatus and targeted to periaxonal membranes. In adult mice, occasional Schwann cells myelinated axons possibly with the aid of endocytic removal of mistargeted P_0. These results indicate that P_0 gene multiplication causes P_0 mistargeting to mesaxon membranes, and through obligate P_0 homophilic adhesion, renders these dynamic membranes inert and halts myelination.

Key words: PNS myelination • homophilic adhesion • dysmyelination • cell polarity • myelin protein gene dosage

Introduction

Myelinating Schwann cells polarize their surface membranes into functionally and molecularly distinct membrane domains (Trapp et al., 1995). Initially, there are two principle domains. The abaxonal plasma membrane is exposed to and interacts with the external environment or endoneurial fluid. The adaxonal or periaxonal membrane is in direct contact with the axon. Myelination is initiated by the spiral wrapping of the Schwann cell mesaxon membranes around the axon. Mesaxon membranes connect the periaxonal and abaxonal membranes and are ultrastructurally characterized by a 12–14-nm gap between their extracellular leaflets and Schwann cell cytoplasm separating their cytoplasmic leaflets (Trapp and Quarles, 1982). Once the mesaxon spirals upon itself two to six times, the periodicity of most mesaxonal membrane converts to compact myelin; extracellular leaflets are separated by a 2.5-nm gap and the cytoplasmic leaflets appear fused (Peters et al., 1991).

Concomitant with the changes in periodicity of mesaxon membranes to compact myelin are molecular changes in the membranes. Periaxonal and mesaxon membranes are enriched in the myelin-associated glycoprotein (MAG)[1], a type I transmembrane glycoprotein with five immunoglobulin-like domains and a molecular weight of ~100 kD. MAG is not detected in compact myelin or the abaxonal membranes of myelinating Schwann cells (Trapp and Quarles, 1982). P_0 protein, the major structural protein of compact PNS myelin (Trapp et al., 1981) is another type I glycoprotein with a single immunoglobulin-like domain and molecular weight of 30 kD. While precise mechanisms by which mesaxon membranes convert to compact myelin are unknown, membrane insertion of P_0 and its subsequent homophilic binding in both trans and cis orientations may exclude MAG and result in compact myelin formation (Heath et al., 1991; Shapiro et al., 1996). MAG and P_0 are sorted into separate carrier vesicles as they exit the trans-Golgi network (Trapp et al., 1995). These vesicles are transported along the myelin internode in a microtubule (MT)-dependent manner, and then inserted directly into the appropriate membrane domain. This site-specific

Address correspondence to Dr. Bruce D. Trapp, Department of Neurosciences, NC30, Lerner Research Institute, Cleveland Clinic Foundation, 9500 Euclid Avenue, Cleveland, OH 44195. Tel.: (216) 444 7177. Fax: (216) 444 7927. E-mail: trappb@ccf.org

[1]*Abbreviations used in this paper:* CMT1A, Charcot-Marie-Tooth disease type 1A; CMT1B, Charcot-Marie-Tooth disease type 1B; CNP, 2′,3′ cyclic nucleotide 3′-phosphodiesterase; MAG, myelin-associated glycoprotein; MDL, major dense line; MT, microtubule; P_0^{tg}, TgN22Mes transgenic mice overexpressing P_0 proteins; PLP, proteolipid protein; PMP22, peripheral myelin protein 22 kD; WT, wild-type.

targeting of P_0 and MAG plays an important role in establishing the polarity and expansion of Schwann cell membranes (Heath et al., 1991; Trapp et al., 1995).

Myelinating Schwann cells can synthesize several square millimeters of surface membranes. This requires high-level transcription of myelin protein genes and precisely regulated doses of translated proteins. Natural and induced myelin protein gene duplications cause dysmyelination and often more severe phenotypes than null mutations in the same gene, indicating the functional importance of appropriate myelin protein gene dosage during myelination. Proteolipid protein (PLP), an integral membrane protein with five membrane-spanning domains, is the major structural protein of CNS myelin (Lees and Brostoff, 1984). Duplications in PLP cause Pelizaeus-Merzbacher disease (Hodes and Dlouhy, 1996), an often fatal dysmyelinating condition of humans. PLP overexpression in transgenic mice also causes dysmyelination (Kagawa et al., 1994; Readhead et al., 1994). Peripheral myelin protein of 22 kD (PMP22) has four membrane-spanning domains and is enriched in PNS myelin (Snipes et al., 1992). Reciprocal unequal crossovers of a 1.5 megabase region of chromosome 17p11.2 causes allelic duplication or deletion of the PMP22 gene (Chance et al., 1994). Allelic duplication of 17p11.2 causes Charcot-Marie-Tooth Disease type 1A (CMT1A), a human peripheral neuropathy characterized by hypomyelination, demyelination/remyelination, onion bulb formation, and axonal atrophy (Lupski et al., 1991; Matsunami et al., 1992). Hereditary neuropathy with liability to pressure palsy (HNPP) is associated with allelic deletion of 17p11.2 (Chance et al., 1993). Alteration in PMP22 gene dosage in rodents also causes peripheral neuropathies (Magyar et al., 1996; Sereda et al., 1996) and supports altered PMP22 gene dosage as the causative factor in CMTIA and HNPP.

P_0 gene duplication has not been associated with human peripheral neuropathies. P_0 missense mutations, however, cause a variety of clinically defined human peripheral neuropathies including CMTIB, Dejerine-Sottas syndrome, and congenital hypomyelination (Warner et al., 1996). P_0 null mutations in mice also cause dysmyelination (Giese et al., 1992). To investigate the potential consequence of increased P_0 gene dosage, several lines of transgenic mice with extra copies of the mouse P_0 gene were generated as described in Wrabetz et al. (2000, this issue). In this report, we have investigated the ultrastructural changes and mechanisms of dysmyelination in the line with highest P_0 mRNA overexpression. Our studies indicate that P_0 accumulates in inappropriate domains of the plasma membrane, blocking spiral mesaxon growth and preventing myelin formation.

Materials and Methods

Generation of Transgenic Mice Overexpressing P_0 Protein Gene

The mP_0TOT vector consists of the whole mouse P_0 gene, including 6 kb of the promoter, all the exons and introns, and the natural polyadenylation signal. This vector directs appropriate cell-specific and developmentally regulated expression of a lacZ reporter gene (Feltri et al., 1999). Generation of transgenic mice carrying the mP_0TOT is described in detail in Wrabetz et al. (2000, this issue). In brief, eight founders were produced that expressed the transgene in peripheral nerve, all displaying varying levels of expression and evidence of peripheral neuropathy including weakness, tremors, and paralysis. Lines were established from three of these founders. This report focuses on the line with the highest level of expression and the most severe neuropathy, TgN22Mes (also referred to as line Tg80.2 in Wrabetz et al., 2000, this issue). For simplicity, throughout the rest of this report the TgN22Mes mice are referred to as P_0^{tg}.

Light and Electron Microscopic Analysis

Mice overexpressing P_0 protein genes and littermate controls were examined at 2, 5, 14, 42, and 90 d of age. They were anesthetized with Metofane and perfused with 4% paraformaldehyde, 2.5% glutaraldehyde, and 0.08 M Sorenson's buffer. Sciatic nerves and lumbar ventral roots were removed, postfixed in osmium tetroxide, and embedded in Epon. For light microscopy, 1-μm thick sections of sciatic nerve were stained with toluidine blue and photographed with a Zeiss Axiophot microscope. For serial section analysis, series of 1-μm thick sections of lumbar ventral roots were mounted in order on slides and stained with toluidine blue. Areas of interest were digitally photographed using a Leica DMLB microscope fitted with an Optronics video camera and image acquisition system. Images were placed in order and aligned on separate layers in Adobe Photoshop 5 software. Profiles of interest were marked and followed by stepping through the layers.

For confocal microscopy, paraformaldehyde-fixed sciatic nerves from 25-d-old mice were teased and immunostained as described (Kidd et al., 1996). The teased fibers were imaged using a Leica TCS-NT confocal microscope.

For EM, thin sections were stained with uranyl acetate and lead citrate, and examined in a Philips CM100 electron microscope.

Electron Microscopic Immunocytochemistry

P_0^{tg} and age-matched wild-type (WT) mice at 5, 14, 42, and 90 d postnatal (three mice per time point) were anesthetized with Metofane and perfused with 2.5% glutaraldehyde, 4% paraformaldehyde, and 0.08 M Sorenson's buffer. The sciatic nerves and L4 ventral roots were removed, infiltrated with 2.3 M sucrose and 30% polyvinylpyrrolidone, placed on specimen stubs, and were then frozen in liquid nitrogen. Ultrathin cryosections (~120-nm thick) were cut on glass knives in a Reichart Ultracut S ultracryomicrotome (Leica Instruments) maintained at −110°C. The sections were placed on carbon- and Formvar-coated grids and immunostained by previously described immunogold procedures (Trapp et al., 1995).

Antibodies

Antibodies used in these studies are well characterized and include: polyclonals directed against P_0 protein (Trapp et al., 1979, 1981), and monoclonals directed against MAG (Doberson et al., 1985; Trapp et al., 1989, 1995), neurofilaments (SMI 31 & 32; Sternberger Monoclonals Inc.), and acetylated α-tubulin (Sigma Chemical Co.). For quantitative immunogold labeling experiments, sections from WT and P_0^{tg} mice were stained in parallel.

Quantitative Analysis of Immunogold Labeling

Ultrathin cryosections were examined and photographed in a Philips CM-100 electron microscope. Digital images were captured from negatives. Gold particles over structures of interest were counted on screen, and areas and distances measured in NIH Image or Photoshop 5 software. Statistical analysis was performed by *t* test. Data are expressed as mean ± SEM. For P_0 labeling of Schwann cell surface membranes, an average of 24 fibers was quantified at each age in both control and P_0^{tg} mice. These fibers were obtained from two control nerves and three P_0^{tg} nerves at each age. This analysis included 76 μm of periaxonal membrane (only 2 d analyzed) and 340 μm of abaxonal membrane in control, and 340 μm of periaxonal membrane and 476 μm of abaxonal membrane in P_0^{tg} cells. An average of 17 endosomes was analyzed at each age in P_0^{tg} mice. In control, 20 and 5 endosomes were analyzed at 5 and 14 d, respectively. Endosomes were not analyzed at 42 and 90 d in control nerves. 36 (control) and 27 (P_0^{tg}) Golgi apparatus were analyzed at 5 d, and 18 (control) and 35 (P_0^{tg}) Golgi apparatus at 42 d. The density of P_0 staining over compact myelin was determined in 25 fibers from 42 d control and P_0^{tg} nerves. These fibers were obtained from three control and three P_0^{tg} nerves.

Results

Several lines of transgenic mice were generated which carried additional copies of the mouse P_0 gene, under control of the native P_0 promoter region. Molecular and morphological features and neurological phenotypes of these mice are described in Wrabetz et al. (2000, this issue). Histologically, the most prominent feature of P_0-overexpressing mice was hypomyelination of peripheral nerves; CNS tissues, which express little or no P_0, appeared unaffected. The degree of neurological impairment correlated with transgene expression and dysmyelination was observed in several lines, indicating that the phenotype was due to overexpression of the P_0 gene and not insertional mutagenesis. The present study investigated the cellular and molecular phenotypes in the line of mice with highest P_0 transgene expression (P_0^{tg}). These mice displayed two consistent phenotypes, failed axonal sorting and arrested myelination.

P_0 Distribution in P_0^{tg} Nerves

Most Schwann cells in P_0^{tg} nerves surrounded single axons or bundles of large diameter axons. To determine if these Schwann cells expressed P_0, teased nerve fibers from 25 d P_0^{tg} nerves were stained with P_0 antibodies and examined by confocal microscopy. Amyelinating Schwann cells surrounding single large diameter axons expressed abundant P_0, had small cell bodies, and were closely spaced along individual axons (Fig. 1 A). P_0 was detected in abaxonal and periaxonal regions of these cells and was concentrated in perikaryal cytoplasm. P_0^{tg} Schwann cells that surrounded bundles of axons also expressed abundant P_0 (Fig. 1 B). This observation suggests that P_0 overexpression impedes the sorting of axons into individual ensheathments.

To investigate whether the same axon/Schwann cell relationships were maintained for the length of individual axons, serial 1-μm sections from 42 d ventral roots were digitally photographed, and individual axons followed

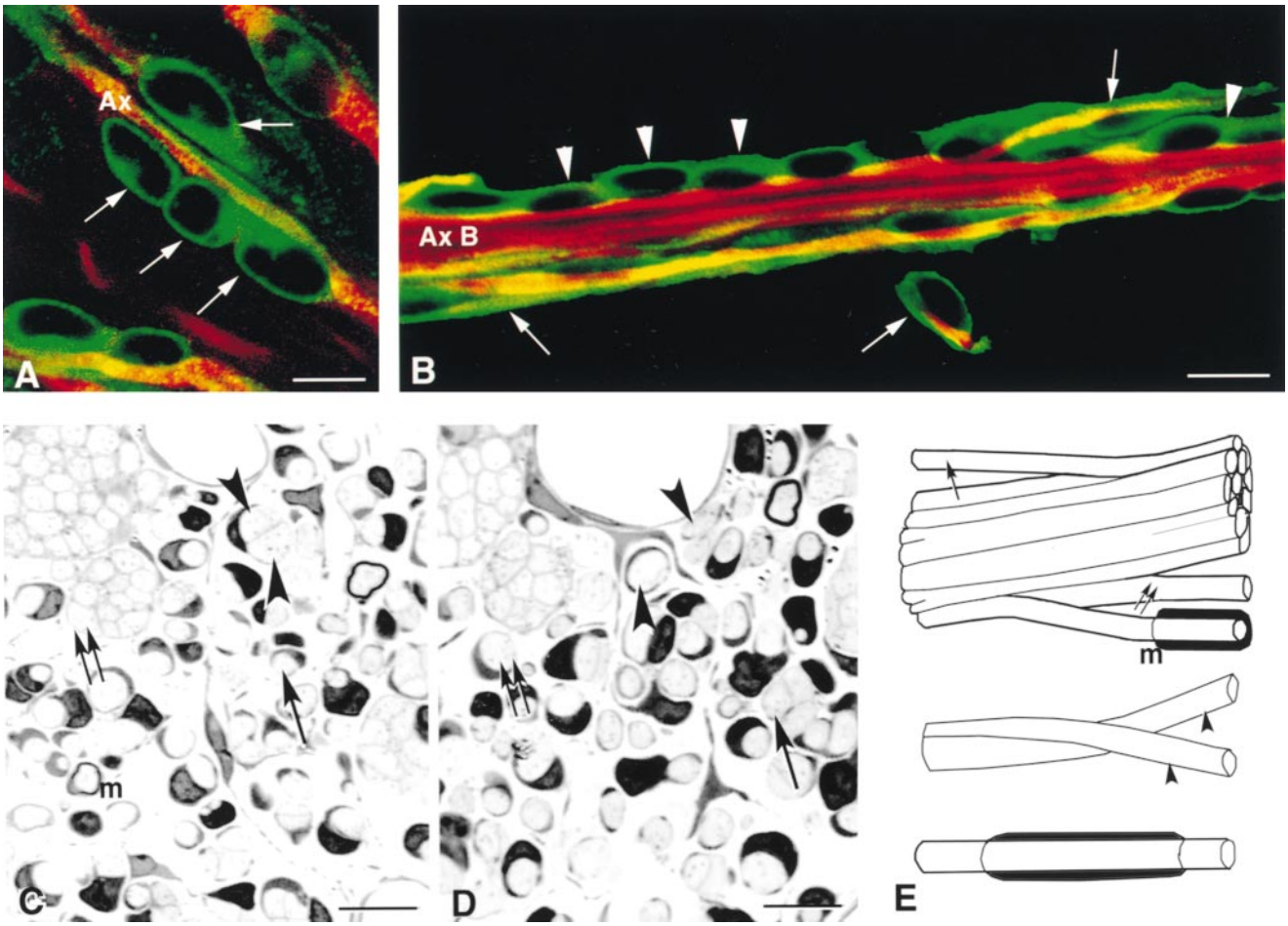

Figure 1. P_0^{tg} Schwann cells express P_0, fail to grow longitudinally, and develop asynchronously along single axons. Confocal micrographs of teased fibers from 25 d P_0^{tg} nerves (A and B) immunostained with P_0 (green) and tubulin (red). Schwann cells associated with single (A and B, arrows) or bundled (B, arrowheads) axons express P_0 protein, but do not myelinate. C and D are identical fields from a set of 50 serial sections (1-μm thick) from a 42 d P_0^{tg} nerve. E is a schematic reconstruction of axonal profiles in the serial sections. Two adjacent axons (C and D, arrowheads) diverge and attain one-to-one contacts with Schwann cells. Others (C and D, arrows) leave one-to-one ensheathments and join large bundles: the reverse also occurs (C and D, paired arrows). One axon exits a bundle, attains a one-to-one relationship with Schwann cells, and then becomes myelinated by another Schwann cell (E, m). Bars, 25 μm.

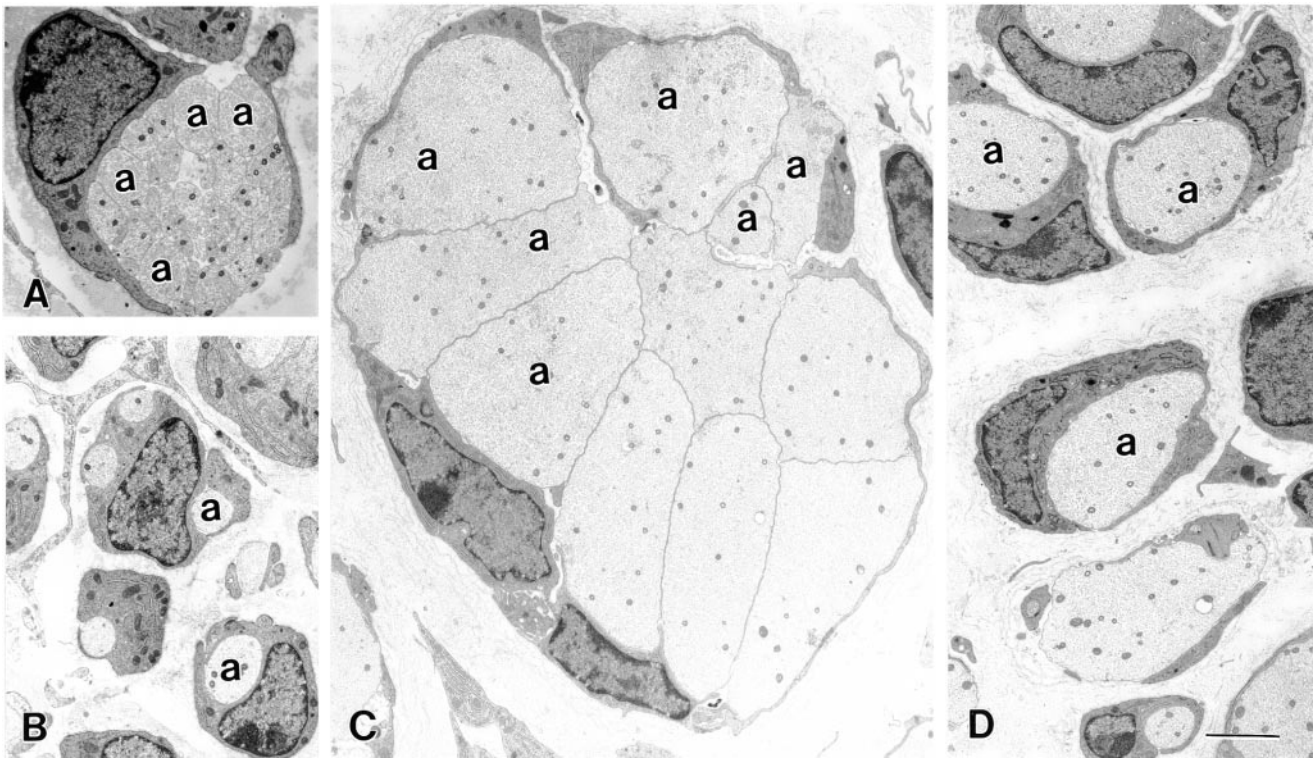

Figure 2. P_0^{tg} Schwann cells fail to sort axons or form myelin. Electron micrographs of P_0^{tg} nerves from 5- (A and B) and 90- (C and D) d-old mice. P_0^{tg} Schwann cells surround, but rarely extend process into, bundles of axons at both ages (A and C). Diameter of bundled axons increased dramatically between 5- (A) and 90- (C) d. Many P_0^{tg} Schwann cells attain one-to-one relationships with axons but fail to form myelin (B and D). a, Axon. Bar, 2 μm.

through 50–100 μm. Axon bundles split into smaller arrangements or combined to form larger bundles (Fig. 1, C, D, and E). Axons were observed to leave a bundle, achieve one-to-one contact with a Schwann cell and then join another (or the same) bundle. No obvious changes in axon diameter marked the transition from large bundles to smaller bundles or to one-to-one ensheathment. The diameters of myelinated and nonmyelinated segments of the same axon did not appear to differ significantly. There was no obvious proximal-to-distal preference in Schwann cell–axon associations (Fig. 1 E). In unmyelinated fibers, P_0^{tg} Schwann cell nuclei were often spaced 1–3 μm apart. In contrast, in WT nerves, nuclei of nonmyelinating (Remak) Schwann cells were 50 μm or more apart, and the nuclei of myelinated Schwann cells were 200–1,000 μm apart.

EM analysis confirmed the phenotypes of failed axonal sorting and arrest of myelination in P_0^{tg} nerves (Fig. 2). At early stages of nerve development (five days), axons that failed to sort in one-to-one relationships were tightly bundled and totally or partially surrounded by Schwann cells (Fig. 2 A). A basal lamina often surrounded the outer perimeter of unensheathed regions of axon bundles, indicating former Schwann cell ensheathment. Myelin was not detected around axons in one-to-one relationships with Schwann cells, and occasionally individual Schwann cells were associated with two axons (Fig. 2 B). These phenotypes predominated in 90 d P_0^{tg} nerves (Fig. 2, C and D). Many axons that failed to sort in one-to-one Schwann cell relationships had diameters in excess of 1 μm, and therefore should have been myelinated.

At all ages analyzed by EM, perinuclear cytoplasm of P_0^{tg} Schwann cells contained the usual complement of organelles and did not display substantial lipid vacuoles, swollen ER, abnormal appearing Golgi apparatus, or apoptotic changes that would indicate that the Schwann cells were dying. Myelin degeneration, debris-laden macrophages, and onion bulbs were not observed in P_0^{tg} or WT nerves.

P_0 Is Mistargeted in P_0^{tg} Schwann Cells

The correlation between extra copies of the P_0 gene and arrest of myelination suggests that overexpression of P_0 protein is responsible for the phenotype. To investigate this and elucidate the possible mechanism, the ultrastructural distribution of P_0 protein was compared in ultrathin cryosections of control and P_0^{tg} nerves. In 2-d WT nerves, P_0 antibodies labeled compact myelin, but not Schwann cell periaxonal, mesaxonal, or abaxonal membranes (Fig. 3 A). In P_0^{tg} nerves, however, intense P_0 labeling of Schwann cell periaxonal, mesaxon, and abaxonal membranes was detected (Fig. 3 B). P_0 labeling of axons and Schwann cell nuclei was rare in both control and P_0^{tg} nerves.

Cryosections from 2, 5, 14, 42, and 90 d control and P_0^{tg} nerves were stained with P_0 antibodies and gold particle densities were quantified per linear length of the periax-

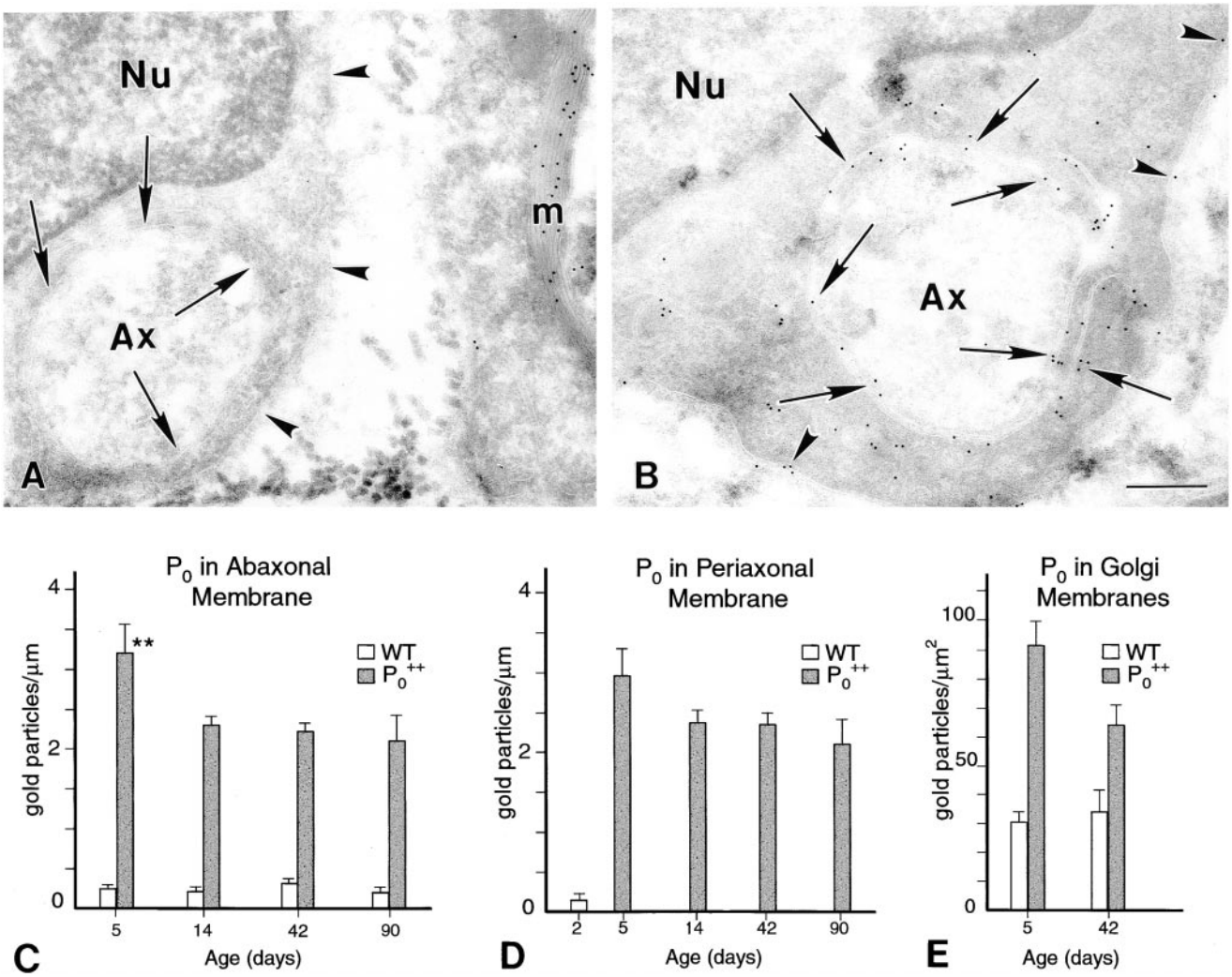

Figure 3. P_0 is mistargeted in P_0^{tg} Schwann cells with arrested myelination. Immunogold labeling in WT Schwann cells at 2 d detected P_0 in compact myelin (A, m), but not in periaxonal membranes (A, arrows), mesaxons, or abaxonal membranes (A, arrowheads). In P_0^{tg} Schwann cells with arrested myelination, P_0 labeling is abundant in the periaxonal (B, arrows), mesaxonal, and abaxonal (B, arrowheads) membranes. Gold particles were quantified and expressed per linear micrometer of abaxonal (C) and periaxonal membrane (D), and per micrometer squared of Golgi apparatus (E) at several ages (mean ± SEM). *t* tests indicated that the density of P_0 was significantly increased ($P < 0.0001$) in P_0^{tg} membranes at all ages (C, D, and E). In addition, P_0 labeling of 5 d P_0^{tg} periaxonal membranes was significantly greater than P_0^{tg} periaxonal membranes at 14, 42, and 90 d (C, $P < 0.0001$). Periaxonal P_0 labeling cannot be scored after compact myelin forms, so WT values were only obtained at 2 d (D). Bar, 0.25 μm.

onal and abaxonal membrane (Fig. 3, C and D). Because of the rapid rate of myelination and the close proximity of compact myelin and periaxonal membranes in control nerves, P_0 gold particles could only be reliably quantified over periaxonal membranes in Schwann cells that had not formed compact myelin at two days. In Schwann cells from control nerves, the labeling indices of two day periaxonal membranes and 2, 5, 14, 42, and 90 d abaxonal plasma membrane ranged from 0.17–0.33 gold particles/μm (not statistically different). The data are consistent with previous reports describing low or undetectable levels of P_0 in these membranes during normal myelination (Trapp et al., 1981). In contrast, the periaxonal and abaxonal membrane of P_0^{tg} Schwann cells that attained one-to-one relationships with axons but failed to myelinate, contained 10–20 times more P_0 labeling than WT fibers (Fig. 3 C). The similarity between the labeling indices of periaxonal and abaxonal membrane suggests constitutive insertion of P_0 into all surface membranes with arrested myelination in P_0^{tg} mice.

The possibility that Golgi membrane-associated P_0 protein is increased in P_0^{tg} Schwann cells was investigated by quantifying the number of gold particles associated with Golgi membranes and their associated vesicles in 5 and 42 d control and P_0^{tg} Schwann cells with arrested myelination (Fig. 3 E). Gold particles were expressed per micrometer squared of Golgi apparatus area. At five days, there was a threefold increase in P_0 gold particles (30.4 vs. 91.6) in P_0^{tg} Schwann cell Golgi membranes, when compared with five-day WT Golgi membranes. This difference was statistically significant ($P < 0.0001$). At 42 d, P_0 labeling of control Schwann cell Golgi apparatus (35.1 gold par-

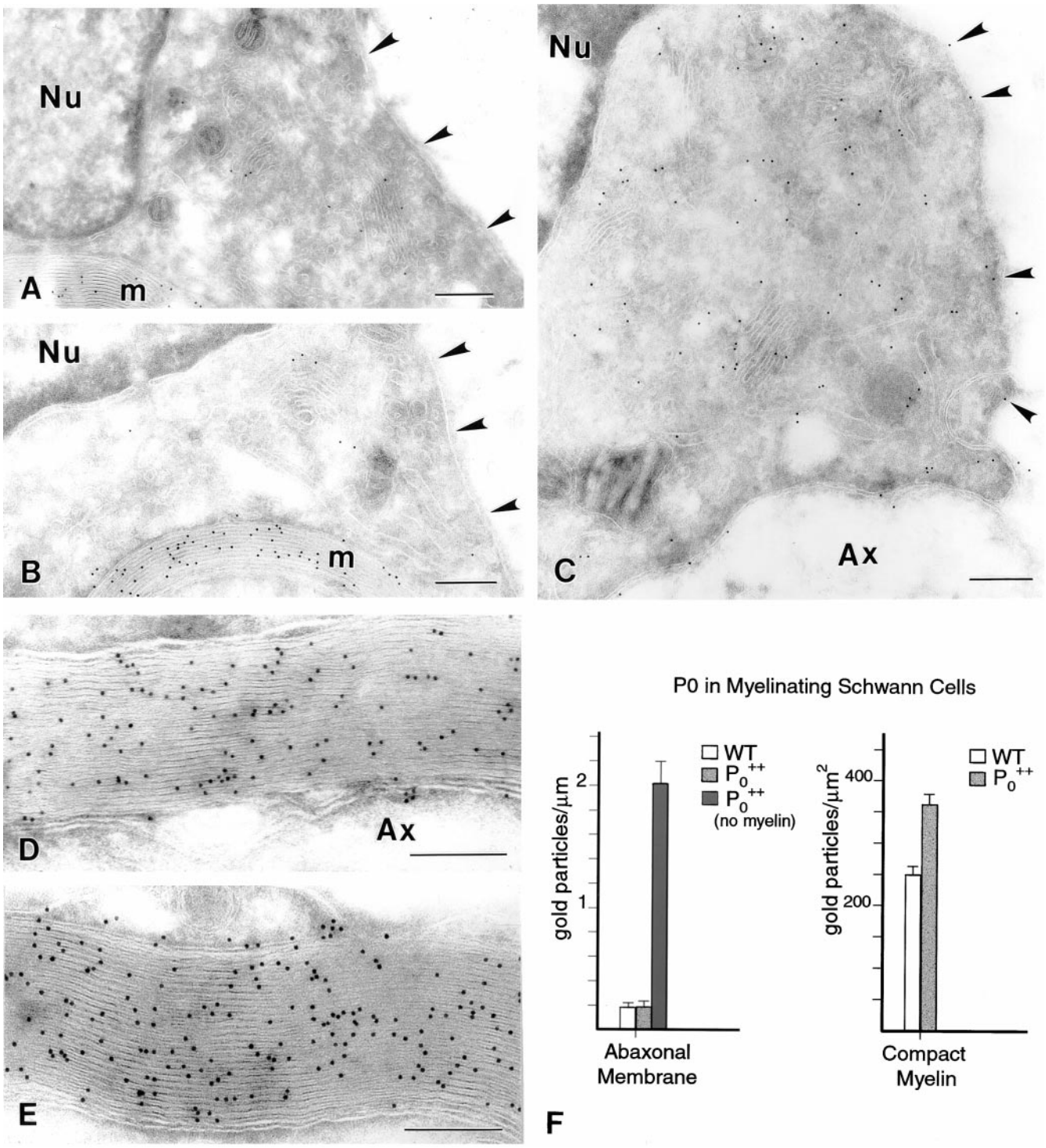

Figure 4. P_0 is correctly targeted in myelinating Schwann cells from 45 d P_0^{tg} nerve. P_0 immunogold labeling of myelinating Schwann cells from WT (A) and P_0^{tg} (B) ventral roots. P_0 is concentrated in compact myelin (A and B, m), but little P_0 is detected on the abaxonal plasma membrane (A and B, arrowheads). In contrast, myelination-arrested Schwann cells have abundant P_0 staining of the abaxonal membrane (C, arrowheads). P_0 labeling of myelination-arrested P_0^{tg} Schwann cell abaxonal membranes was significantly increased ($P < 0.0001$, *t* test) compared with abaxonal membranes in myelinating P_0^{tg} and WT Schwann cells (F). Compact myelin appears ultrastructurally similar in WT (D) and P_0^{tg} internodes (E). P_0 labeling of compact myelin was significantly increased ($P < 0.0001$) in P_0^{tg} nerves (F). Bars, 1 μm.

ticles/μm^2) was similar to that at five days and ~45% less ($P < 0.01$) than that found in 42 d P_0^{tg} Schwann cells (66.9 gold particles/μm^2).

Some Schwann cells in P_0^{tg} nerves escaped the inhibition of myelination and formed compact myelin, suggesting that these cells may have established normal targeting pathways for P_0. P_0 labeling indices for the abaxonal membrane of these P_0^{tg} myelinating Schwann cells were identi-

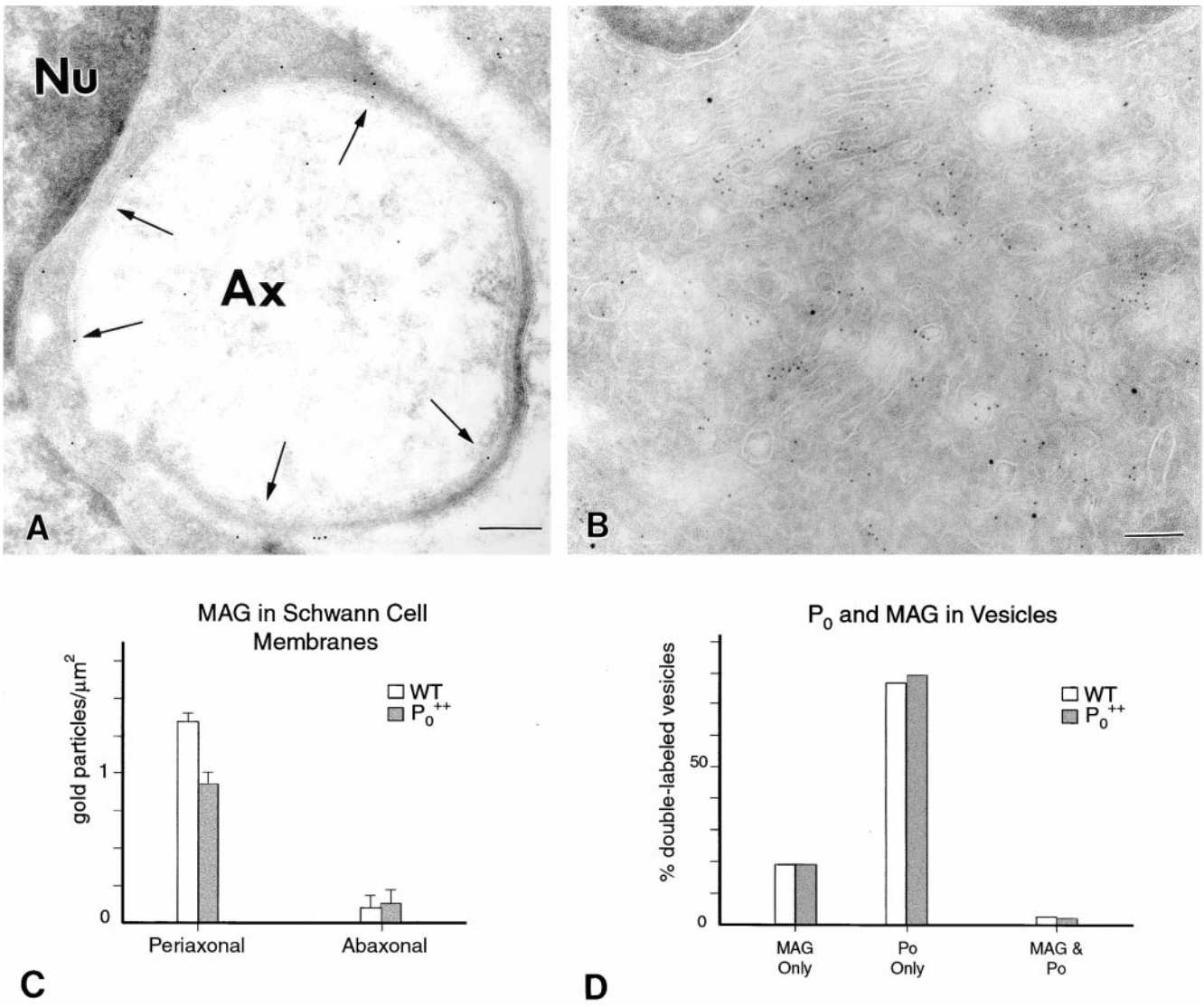

Figure 5. MAG is appropriately targeted and sorted in P_0^{tg} Schwann cells. A, P_0^{tg} Schwann cells with arrested myelination contain MAG labeling in periaxonal membranes. Periaxonal MAG labeling was slightly reduced in 5-d-old P_0^{tg} Schwann cells when compared with WT Schwann cells (C). Abaxonal membranes contained little MAG labeling in WT and P_0^{tg} Schwann cells (C). In ultrathin cryosections from 5-d-old mice double-labeled with P_0 (B, 5-nm gold) and MAG (B, 10-nm gold) antibodies, 80% of Golgi apparatus-associated vesicles were labeled P_0 antibodies, 19% by MAG antibodies, and <2% with P_0 and MAG. Ax, Axon; Nu, nucleus. Bars, 1 μm.

cal (0.2 particles/μm) to age-matched WT fibers (Fig. 4, A and B) and tenfold less than those detected in nonmyelinating P_0^{tg} Schwann cells in the same sections (Figs. 3, C and D, 4 C). When P_0 labeling over compact myelin was compared in controls (Fig. 4 D) and P_0^{tg} mice (Fig. 4 E), the labeling index was ~40% higher for P_0^{tg} internodes (358 vs. 251 gold particles/μm^2). This observation argues against the complete silencing of the P_0 transgene in Schwann cells that myelinate in P_0^{tg} nerves.

MAG Sorting and Targeting Is Unaffected by P_0 Overexpression

Overexpression and mistargeting of P_0 may also affect the sorting and targeting of MAG, which is enriched in periaxonal and mesaxon membranes and excluded from compact myelin and the Schwann cell abaxonal membrane (Trapp and Quarles, 1982; Trapp et al., 1995). Immunogold experiments were performed to determine if MAG was appropriately targeted in P_0^{tg} Schwann cells. As in WT myelinating cells, MAG antibodies labeled Golgi membranes and cytoplasmic vesicles of myelination-arrested P_0^{tg} Schwann cells (Fig. 5 A), indicating that the protein was synthesized and processed in these cells. When MAG labeling indices were compared in five day WT and P_0^{tg} nerves (Fig. 5 B), abaxonal membrane MAG staining was low (<0.2 particles/μm) in both control and P_0^{tg} nerves (Fig. 5 C). In contrast, the periaxonal membrane of control and P_0^{tg} fibers contained 1.3 and 1.0 gold particles/μm (Fig. 5 C). Whereas P_0 overexpression slightly reduced the amount of periaxonal MAG, it had no apparent effect on the targeting of MAG to the periaxonal membrane. MAG labeling was rare in Schwann cell nuclei or axons.

P_0 and MAG are sorted into separate carrier vesicles as

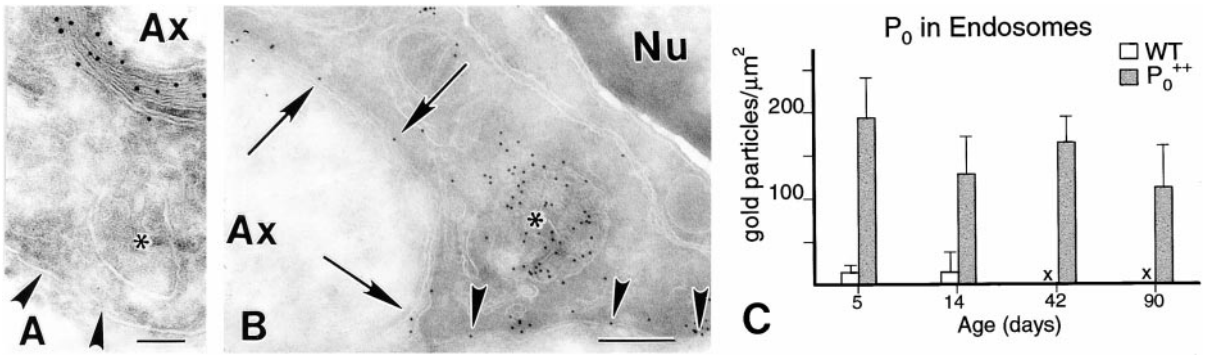

Figure 6. P_0 is targeted to endosomes in P_0^{tg} Schwann cells with arrested myelination. In ultrathin cryosections of myelinating Schwann cells from control nerves, endosomes (A*) were rarely labeled by P_0 antibodies. In contrast, endosomes in P_0^{tg} Schwann cells with arrested myelination (B*) were abundant and intensely labeled by P_0 antibodies. P_0 labeling per endosomal area was quantified in control myelinating Schwann cell and P_0^{tg} Schwann cells with arrested myelination. P_0^{tg} endosomes contained 10–100 times greater P_0 than endosomes in control Schwann cells (5 and 14 d, $P < 0.0001$ in *t* tests). Myelinating Schwann cells in 42- and 90-d WT nerves had too few endosomes for statistical analysis (C, x). *, Endosomes; Ax, axon; Nu, nucleus. B, Arrows denote periaxonal membrane and arrowheads denote abaxonal membrane. Bars: (A) 0.1 μm; (B) 0.25 μm.

they exit the trans-Golgi network (Trapp et al., 1995). To determine if P_0 overexpression alters P_0 or MAG sorting, cryosections from five day mice were labeled with both P_0 and MAG antibodies, and gold particles associated with vesicles in the area of the trans-Golgi network (Fig. 5 B) were quantified (Fig. 5 C) as MAG-positive, P_0-positive, or MAG–P_0-positive. As described previously in control nerves (Trapp et al., 1995), ~80% of vesicles in P_0^{tg} Schwann cells contained only P_0 gold particles (5 nm), 19% contained only MAG gold particles (10 nm), and 1–2% contained both MAG and P_0 (5- and 10-nm gold particles). In both control and P_0^{tg} Schwann cells, ~65% of the P_0-labeled vesicles contained more than one gold particle. These data indicate that MAG and P_0 are appropriately sorted into separate carrier vesicles as they exit the trans-Golgi network of P_0^{tg} Schwann cells with arrested myelination.

P_0 Is Abnormally Enriched in Endosomes in P_0^{tg} Schwann Cells

Abundant P_0 labeling of transport vesicles and normal appearance of RER and Golgi membranes suggested that P_0 protein was appropriately synthesized and processed in P_0^{tg} Schwann cells with arrested myelination. However, P_0 labeling indices of Schwann cell surface membranes remained relatively constant between 14 and 42 d (Fig. 3, C and D). These observations suggest a rapid turnover of P_0 from P_0^{tg} Schwann cell surface membranes, possibly by endocytosis and P_0 degradation through the endosomal/lysosomal system. This hypothesis was tested by comparing the density of gold particles over endosomes in P_0-stained cryosection from control and P_0^{tg} Schwann cells at 5, 14, 42, and 90 d (Fig. 6). At five days, endosomes were prominent in P_0^{tg} Schwann cells with arrested myelination (Fig. 6 B). Endosomes were less conspicuous in control Schwann cells (Fig. 6 A). Quantification of P_0 labeling detected 10 gold particles/μm^2 of endosomal area in control Schwann cells. In contrast, P_0^{tg} Schwann cells contain 191 gold particles/μm^2 of endosome area. At 14 d, endosomes in P_0^{tg} Schwann cells contained 129 gold particles/μm^2, compared with 12 gold particles/μm^2 in control Schwann cells. At 42 and 90 d, endosomes in P_0^{tg} Schwann cells contains 152 and 101 gold particles/μm^2. Endosomes were rare in control Schwann cells of the same ages and, when present, contained >1 gold particle/μm^2. These data are consistent with continuous removal of mistargeted P_0 in P_0^{tg} Schwann cells with arrested myelination.

Mistargeted P_0 Disrupts the Mesaxon

Mesaxon membranes spiral upon themselves during initial stages of myelination. They initially form 3–6 spiral wraps, which contain detectable levels of MAG, but not P_0 protein (Trapp, 1988). The periodicity of portions of these mesaxon membranes then changes to that of compact myelin: extracellular leaflets are separated by a 2.5-nm gap and cytoplasmic leaflets appear as a fused major dense line (MDL). At this stage, P_0 protein is detectable in single MAG-negative compact myelin lamellae (Trapp, 1988). These observations are consistent with the hypothesis that mesaxon membranes are dynamic migratory membranes and that the insertion of P_0 protein into these mesaxon membranes excludes MAG and favors homophilic binding between the extracellular domains of P_0 in both cis and trans orientations, resulting in the 2.5-nm periodicity of compact myelin. Analysis of the periodicity of P_0^{tg} and control Schwann cell periaxonal and mesaxonal membranes provides an opportunity to test this hypothesis. The normal 12–14 nm spacing between the extracellular leaflets of periaxonal membrane and axolemma, and between apposing mesaxon membranes are shown in a control fiber (Fig. 7, A and B). In P_0^{tg} Schwann cells (Fig. 7, C and D), the periaxonal space is similar to that in control fibers (12–14 nm). However, the extracellular leaflets (Fig. 7 D) of the mesaxon wraps are separated by a smaller gap resembling that of compact myelin. This compact myelin-like separation of the extracellular leaflets of this mesaxon was documented in most P_0^{tg} Schwann cells with arrested myelination. The length of these P_0 containing mesaxon membranes varies from short outer mesaxon-like structures that connect periaxonal and plasma membranes (Fig.

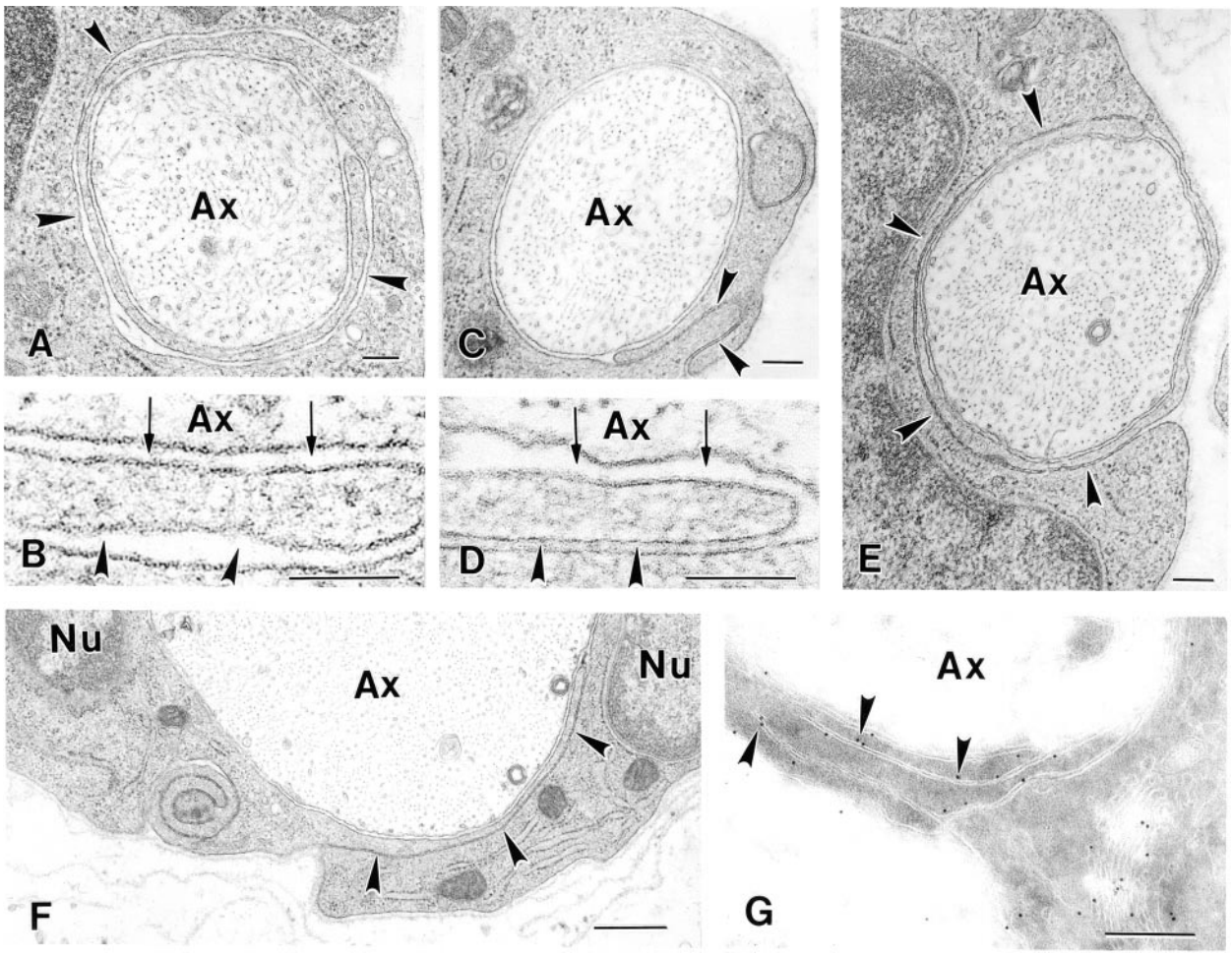

Figure 7. P_0 mistargeting alters the spacing between Schwann cell membranes. A–E compare early mesaxon formation in control (A and B) and P_0^{tg} (C, D, and E) fibers. The spacing between apposing Schwann cell mesaxon membranes (B and D, arrowheads) averages 12–14 nm in control (B, arrowheads) and resembles that of compact myelin in P_0^{tg} (D, arrowheads). Spacing between Schwann cell periaxonal membranes and the axons were similar in control and P_0^{tg} fibers (B and D, arrows). Mesaxon membranes in P_0^{tg} nerves rarely encircled >50% of the axon (E). Abaxonal membranes of adjacent P_0^{tg} Schwann cells occasionally excluded their basal lamina and were closely apposed (F, arrowheads). Closely apposed mesaxon and abaxonal membranes were labeled by P_0 antibodies (G, arrowheads). Ax, Axon; Nu, Schwann cell nuclei. Bars: (A, C, E, and G) 0.2 μm; (B and D) 0.1 μm; (F) 0.5 μm.

7 C) to 50% ensheathment of axonal perimeter (Fig. 7 E). Similarly, where the abaxonal membrane of two adjacent P_0^{tg} Schwann cells were closely apposed, the basal lamina was excluded and the extracellular leaflets were separated by distances reminiscent of the periodicity of compact myelin (Fig. 7 F, arrowheads). The mesaxon membranes with closely apposed extracellular leaflets were stained by P_0 antibodies (Fig. 7 G).

Discussion

This report describes arrest of myelination and failed axon sorting due to overexpression of P_0 protein. Our data established that P_0 protein is overexpressed in mesaxon membranes where its obligate homophilic adhesion arrests myelination. While molecular mechanisms responsible for failed axonal sorting were not investigated in detail, Schwann cells that fail to sort axons express excessive levels of P_0. Early, high level P_0 expression in developing Schwann cells inhibits the polarization of Schwann cell membranes into appropriate functional domains and the dynamic axonal interaction and Schwann cell membrane expansion required for appropriate axonal sorting and myelination.

Specificity of Phenotype

Axon–Schwann cell interactions and signaling are bidirectional and mediated by physical contact. Unidentified axonal signals initiate a myelinating genome in Schwann cells and axonal contact is essential for myelin formation (Aguayo et al., 1976; Weinberg and Spencer, 1976). Schwann cells in turn provide an extrinsic trophic effect for maturation of the axon (Windebank et al., 1985; deWaegh et al., 1992; Hsieh et al., 1994; Sanchez et al., 1996; Yin et al., 1998). Individual axons in P_0^{tg} mice can be myelinated, surrounded by a Schwann cell with arrested myelination, or part of an axonal bundle (Fig. 1 E). These

observations and the rescue of the P_0^{tg} phenotype through breeding to P_0 null mice (Wrabetz et al., 2000, this issue) are most consistent with a primary Schwann cell defect in P_0^{tg} mice. While extensive analysis of axonal diameters has yet to be performed, axonal diameters increase in the P_0^{tg} nerves regardless of the Schwann cell state of differentiation. Schwann cells in one-to-one associations with axons contained MAG, a molecule previously demonstrated to influence axonal maturation by increasing the phosphorylation state and spacing of neurofilaments (Yin et al., 1998).

P_0 Overexpression Causes a Unique Phenotype

Myelin protein overexpression causes a variety of phenotypes in mice. Whereas Schwann cells overexpressing P_0 share some similarities with Schwann cells overexpressing other myelin proteins, the phenotype of failed axonal sorting and arrest of myelination at early mesaxon formation is unique. The P_0^{tg} phenotype differs from that produced by the toxic accumulation of overexpressed PLP in the Golgi apparatus and RER (Kagawa et al., 1994; Readhead et al., 1994). Schwann cell death and abnormal RER and Golgi networks were not observed in P_0^{tg} nerves. Processing and folding the four membrane-spanning PLP in the RER and Golgi apparatus may represent a greater challenge than the processing of the single membrane spanning P_0 protein. Transgenic mice with extra copies of PMP22 genes display progressive neurological phenotypes and peripheral nerve pathology that correlate with copy number (Magyar et al., 1996; Sereda et al., 1996). At higher doses, Schwann cells sorted axons in one-to-one relationships, formed a normal basal lamina, rarely formed myelin, but had normal mesaxon membrane spacing. Although the function of PMP22 is unknown, the mechanisms responsible for arrest of myelination in PMP22 overexpressing mice are likely to differ significantly from those in P_0^{tg} mice.

2′,3′ cyclic nucleotide 3′-phosphodiesterase (CNP) is an extrinsic membrane protein that associates with the cytoplasmic side of oligodendrocyte and Schwann cell surface membranes, but is normally excluded from compact myelin (Yin et al., 1997; Braun et al., 1988; Trapp et al., 1988). In transgenic mice with a sixfold increase in CNP levels (Gravel et al., 1996; Yin et al., 1997), oligodendrocytes spirally wrapped axons, but often failed to form MDL. CNP was mistargeted to the cytoplasmic leaflet of these myelin membranes and prevented normal accumulation of myelin basic protein (Yin et al., 1997), a molecular requirement of MDL formation in the CNS (Privat et al., 1979; Roach et al., 1983). These observations provide another example of mistargeting of a myelin-related protein due to overexpression and indicate protein-specific phenotypes as a result of the molecular properties of the overexpressed proteins.

Mechanism of P_0 Targeting

Much of what is known about mechanisms of protein sorting and targeting has been obtained from in vitro studies of epithelial cells that polarize their surfaces into apical and basolateral domains (Rodriguez-Boulan and Nelson, 1989; Simons and Wandinger-Ness, 1990; Mostov et al., 1992; Weimbs et al., 1997). Proteins are targeted to appropriate domains by direct or indirect pathways (Rindler et al., 1984; Hubbard and Stieger, 1989). Previous studies support direct delivery of P_0 protein to compact myelin in an MT-dependent manner (Trapp et al., 1995; Kidd et al., 1996). In the present study, P_0 protein was detected on all surface membranes of P_0^{tg} Schwann cells, indicating that P_0 is synthesized and transported, but not appropriately targeted. The distributions of Golgi apparatus, intermediate filaments, RER, and smooth ER are maintained by MTs (Trapp et al., 1995) and appeared unaltered in P_0^{tg} Schwann cells. Based on these observations, it is unlikely that P_0 mistargeting results from abnormal MT distribution or function.

P_0^{tg} Schwann cells in one-to-one relationship with axons appropriately ensheath axons, target MAG to periaxonal membranes, and form a basal lamina on their abaxonal membrane. Thus, a significant degree of membrane polarization and appropriate protein targeting occurs in the presence of P_0 overexpression. Site-specific targeting of membrane proteins occurs via a variety of mechanisms including sorting into specific transport vesicles in the Golgi apparatus, site-specific intracellular vesicular transport, site-specific vesicle docking or fusion, inhibition of vesicle docking or fusion, and stabilization of proteins within discrete membrane domains (Weimbs et al., 1997; Allan and Balch, 1999). Whereas our data indicated normal sorting of P_0 and MAG in the trans-Golgi network, we cannot rule out the possibility that excessive P_0 is missorted into vesicles destined for membranes other than compact myelin. P_0 labeling of Golgi membranes was increased in P_0^{tg} Schwann cells. P_0 did not accumulate in the Golgi apparatus with age, however, and Golgi membranes appeared normal in electron micrographs. These observations support normal synthesis and processing of P_0 to the carrier vesicle stage. In addition, when carrier vesicle transport is halted in myelinating Schwann cells by MT disruption, P_0-enriched carrier vesicles accumulated in perinuclear cytoplasm and fused to form compact myelin-like membranes (Trapp et al., 1995). Such membranes were not abundant in P_0^{tg} Schwann cells cytoplasm, supporting targeting of P_0 to surface membranes.

Whereas our data supports interpretations regarding the synthesis, sorting, and targeting of P_0, they are based on static images of P_0 distribution. Pulse–chase experiments of P_0 synthesis and degradation would be essential to establish the role of the endosomal system in P_0 targeting (Gu and Gruenberg, 1999; Marsh and McMahon, 1999). While the interpretation that mistargeted P_0 is removed from membranes by endocytosis is supported by the close proximity of P_0-labeled endosomes to abaxonal membranes, it is possible that overexpressed P_0 is also directly targeted to the endosomal/lysosomal system. In either case, the absence of significant amounts of P_0 in endosomes during normal myelination supports the general conclusion that P_0 overexpression results in P_0 accumulation in endosomes.

P_0 Homophilic Binding Inhibits Mesaxon Expansion

During normal myelination, P_0 has been detected in compact myelin, but not mesaxon membranes. As mesaxon

membranes convert to compact myelin, however, P_0 is likely to be transiently present in MAG-positive mesaxon membranes at levels not detected by current techniques. In P_0^{tg} mesaxon membranes, levels of P_0 reached the threshold for detection and trans adhesion during their initial wrap. Arrest of myelination may result from simple overexpression of P_0 in mesaxon membranes, where it is normally expressed at low undetectable levels on its way to the expanding myelin sheath, or by early expression and mistargeting to mesaxon membranes before establishment of migratory machinery. P_0-mediated trans adhesion at 2.5 nm also requires exclusion of molecules with large extracellular domains. MAG (Fig. 5, A and C) and P_0 (Fig. 3, B and D) were detected in the periaxonal membrane of P_0^{tg} Schwann cells that apposed the P_0-negative axolemma by 12–14 nm (Fig. 7). The abaxonal membrane of most P_0^{tg} Schwann cells contained significant levels of P_0 and a normal appearing basal lamina. The presence of P_0 in a single membrane, therefore, does not exclude other proteins with large extracellular domains. However, when P_0-positive mesaxon or abaxonal membranes apposed each other, MAG and the basal lamina were excluded, resulting in close apposition (2.5 nm; Fig. 7). In addition, P_0 transfection in nonadherent cells in vitro induced obligate adhesion of apposing plasma membranes, reorganization of submembranous cytoskeleton, and junctional complexes at the transition between adherent and nonadherent membrane domains (D'Urso et al., 1990; Filbin et al., 1990). Liquid crystallography at 1.9 Å resolution supports emanation of the extracellular domain of P_0 as cis-linked tetramers that bind to P_0 tetramers in opposite orientation on the apposing membrane surface (Shapiro et al., 1996). Collectively, these data support the possibility that arrest of myelination in P_0^{tg} mice is caused by early trans-P_0 tetramer binding of the initial mesaxon wrap. This trans-P_0 binding induces cis-P_0 tetramer binding, which then excludes molecules responsible for spiral wrapping of mesaxon membranes.

We wish to thank Heide Peickert and Denice Springman for technical assistance, and Vikki Pickett for typing the manuscript.

This work was supported by the National Institutes of Health grants NS-38186 (to B.D. Trapp) and NS-23375 (to A. Messing), by Telethon Italy (L. Wrabetz and M.L. Feltri), European Community Biomed Program (L. Wrabetz), and Fondazione Giovanni Armenise-Harvard (L. Wrabetz and M.L. Feltri).

Submitted: 19 October 1999
Revised: 12 January 2000
Accepted: 24 January 2000

References

Aguayo, A.J., J. Epps, L. Charron, and G.M. Bray. 1976. Multipotentiality of Schwann cells in cross anastomosed and grafted myelinated and unmyelinated nerves: quantitative microscopy and radioautography. *Brain Res.* 104:1–20.

Allan, B.B., and W.E. Balch. 1999. Protein sorting by directed maturation of Golgi compartments. *Science.* 285:63–66.

Braun, P.E., F. Sandillon, A. Edwards, J.-M. Matthieu, and A. Privat. 1988. Immunocytochemical localization by electron microscopy of 2′,3′-cyclic nucleotide 3′-phosphodiesterase in developing oligodendrocytes of normal and mutant brain. *J. Neurosci.* 8:3057–3066.

Chance, P.F., M.K. Alderson, K.A. Leppig, M.W. Lensch, N. Matsunami, B. Smith, P.D. Swanson, S.J. Odelberg, C.M. Disteche, and T.D. Bird. 1993. DNA deletion associated with hereditary neuropathy with liability to pressure palsies. *Cell.* 72:143–151.

Chance, P.F., N. Abbas, M.W. Lensch, L. Pentao, B.B. Roa, P.I. Patel, and J.R. Lupski. 1994. Two autosomal dominant neuropathies result from reciprocal DNA duplication/deletion of a region on chromosome 17. *Hum. Mol. Gen.* 3:223–228.

D'Urso, D., P.J. Brophy, S.M. Staugaitis, C.S. Gillespie, A.B. Frey, J.G. Stempak, and D.R. Colman. 1990. Protein zero of peripheral nerve myelin: biosynthesis, membrane insertion, and evidence for homotypic interaction. *Neuron.* 2:449–460.

deWaegh, S.M., V.M.Y. Lee, and S.T. Brady. 1992. Local modulation of neurofilament phosphorylation, axonal caliber, and slow axonal transport by myelinating Schwann cells. *Cell.* 68:451–463.

Doberson, M.G., J.K. Hammer, A.B. Noronha, T.D. MacIntosch, B.D. Trapp, R.O. Brady, and R.H. Quarles. 1985. Generation and characterization of mouse monoclonal antibodies to the myelin-associated glycoprotein (MAG). *Neurochem. Res.* 10:423–437.

Feltri, M.L., M. D'antonio, A. Quattrini, R. Numerato, M. Arona, S. Previtali, S.Y. Chiu, A. Messing, and L. Wrabetz. 1999. A novel P_0 glycoprotein transgene activates expression of lacZ in myelin-forming Schwann cells. *Eur. J. Neurosci.* 11:1577–1586.

Filbin, M.T., F.S. Walsh, B.D. Trapp, J.A. Pizzey, and G.I. Tennekoon. 1990. The role of myelin P_0 protein as a homophilic adhesion molecule. *Nature.* 344:871–872.

Giese, K.P., R. Martini, G. Lemke, P. Soriano, and M. Schachner. 1992. Mouse P_0 gene disruption leads to hypomyelination, abnormal expression of recognition molecules, and degeneration of myelin and axons. *Cell.* 71:565–576.

Gravel, M., J. Peterson, V.W. Yong, V. Kottis, B. Trapp, and P.E. Braun. 1996. Overexpression of 2′,3′-cyclic nucleotide 3′-phosphodiesterase in transgenic mice alters oligodendrocyte development and produces aberrant myelination. *Mol. Cell. Neurosci.* 7:453–466.

Gu, F., and J. Gruenberg. 1999. Biogenesis of transport intermediates in the endocytic pathway. *FEBS Lett.* 452:61–66.

Heath, J.W., T. Inuzuka, R.H. Quarles, and B.D. Trapp. 1991. Distribution of P_0 protein and the myelin-associated glycoprotein in peripheral nerves from Trembler mice. *J. Neurocytol.* 20:439–449.

Hodes, M.E., and S.R. Dlouhy. 1996. The proteolipid protein gene: double, double, ... and trouble. *Am. J. Hum. Genet.* 59:12–15.

Hsieh, S.-T., G.J. Kidd, T.O. Crawford, Z. Xu, B.D. Trapp, D.W. Cleveland, and J.W. Griffin. 1994. Regional modulation of neurofilament organization by myelination in normal axons. *J. Neurosci.* 14:6392–6401.

Hubbard, A.L., and B. Stieger. 1989. Biogenesis of endogenous plasma membrane proteins in epithelial cells. *Annu. Rev. Physiol.* 51:755–770.

Kagawa, T., K. Ikenaka, Y. Inoue, S. Kuriyama, T. Tsujii, J. Nakao, K. Nakajima, J. Aruga, H. Okano, and K. Mikoshiba. 1994. Glial cell degeneration and hypomyelination caused by overexpression of myelin proteolipid protein gene. *Neuron.* 13:427–442.

Kidd, G.J., S.B. Andrews, and B.D. Trapp. 1996. Axons regulate the distribution of Schwann cell microtubules. *J. Neurosci.* 16:946–954.

Lees, M.B., and S.W. Brostoff. 1984. Proteins of myelin. *In* Myelin. P. Morrell, editor. Plenum Press, New York. 197–224.

Lupski, J.R., R. Montes de Oca-Luna, S. Slaugenhaupt, L. Pentao, V. Guzzetta, B.J. Trask, O. Saucedo-Cardenas, D.F. Barker, J.M. Killian, C.A. Garcia, et al. 1991. DNA duplication associated with Charcot-Marie-Tooth disease type 1A. *Cell.* 66:219–232.

Magyar, J.P., R. Martini, T. Ruelicke, A. Aguzzi, K. Adlkofer, Z. Dembic, J. Zielasek, K.V. Toyka, and U. Suter. 1996. Impaired differentiation of Schwann cells in transgenic mice with increased *PMP22* gene dosage. *J. Neurosci.* 16:5351–5360.

Marsh, M., and H.T. McMahon. 1999. The structural era of endocytosis. *Science.* 285:215–220.

Matsunami, N., B. Smith, L. Ballard, M.W. Lensch, M. Robertson, H. Albertsen, C.O. Hanemann, H.W. Müller, T.D. Bird, R. White, and P.F. Chance. 1992. Peripheral myelin protein-22 gene maps in the duplication in chromosome 17p11.2 associated with Charcot-Marie-Tooth 1A. *Nature Gen.* 1:176–179.

Mostov, K., G. Apodaca, B. Aroeti, and C. Okamoto. 1992. Plasma membrane protein sorting in polarized epithelial cells. *J. Cell Biol.* 116:577–583.

Peters, A., S.L. Palay, and H.d. Webster. 1991. The Fine Structure of the Nervous System: Neurons and their Supporting Cells. Oxford University Press, New York.

Privat, A., C. Jacque, J.M. Bourre, P. Duponey, and N. Baumann. 1979. Absence of the major dense line in myelin of the mutant mouse "Shiverer". *Neurosci. Lett.* 12:107–112.

Readhead, C., A. Schneider, I. Griffiths, and K.-A. Nave. 1994. Premature arrest of myelin formation in transgenic mice with increased proteolipid protein gene dosage. *Neuron.* 12:583–595.

Rindler, M.J., I.E. Ivanov, H. Plesken, E. Rodriguez-Boulan, and D.D. Sabatini. 1984. Viral glycoproteins destined for apical or basolateral plasma membrane domains transverse the same Golgi apparatus during their intracellular transport in Madin-Darby canine kidney cells. *J. Cell Biol.* 98:1304–1319.

Roach, A., K.B. Boylan, S. Horvath, S.B. Prusiner, and L.E. Hood. 1983. Characterization of cloned cDNA representing rat myelin basic protein: absence of expression in brain of *shiverer* mutant mice. *Cell.* 34:799–806.

Rodriguez-Boulan, E., and W.J. Nelson. 1989. Morphogenesis of the polarized epithelial cell phenotype. *Science.* 245:718–725.

Sanchez, I., L. Hassinger, P.A. Paskevich, H.D. Shine, and R.A. Nixon. 1996. Oligodendroglia regulate the regional expansion of axon caliber and local

accumulation of neurofilaments during development independently of myelin formation. *J. Neurosci.* 16:5095–5105.

Sereda, M., I. Griffiths, A. Pühlhofer, H. Stewart, M.J. Rossner, F. Zimmermann, J.P. Magyar, A. Schnieder, E. Hund, H.-M. Meinck, et al. 1996. A transgenic rat model of Charcot-Marie-Tooth disease. *Neuron.* 16:1049–1060.

Shapiro, L., J.P. Doyle, P. Hensley, D.R. Colman, and W.A. Hendrickson. 1996. Crystal structure of the extracellular domain from P_0, the major structural protein of peripheral nerve myelin. *Neuron.* 17:435–449.

Simons, K., and A. Wandinger-Ness. 1990. Polarized sorting in epithelia. *Cell.* 62:207–210.

Snipes, G.J., U. Suter, A.A. Welcher, and E.M. Shooter. 1992. Characterization of a novel peripheral nervous system myelin protein (PMP-22/SR13). *J. Cell Biol.* 117:225–238.

Trapp, B.D. 1988. Distribution of the myelin-associated glycoprotein and P_0 protein during myelin compaction in Quaking mouse peripheral nerve. *J. Cell Biol.* 107:675–685.

Trapp, B.D., and R.H. Quarles. 1982. Presence of the myelin-associated glycoprotein correlates with alterations in the periodicity of peripheral myelin. *J. Cell Biol.* 92:877–882.

Trapp, B.D., L.J. McIntyre, R.H. Quarles, N.H. Sternberger, and H.d. Webster. 1979. Immunocytochemical localization of rat peripheral nervous system myelin proteins: P2 protein is not a component of all peripheral nervous system myelin sheaths. *Proc. Natl. Acad. Sci. USA.* 76:3552–3556.

Trapp, B.D., Y. Itoyama, N.H. Sternberger, R.H. Quarles, and H.d. Webster. 1981. Immunocytochemical localization of P_0 protein in Golgi complex membranes and myelin of developing rat Schwann cells. *J. Cell Biol.* 90:1–6.

Trapp, B.D., L. Bernier, S.B. Andrews, and D.R. Colman. 1988. Cellular and subcellular distribution of 2′,3′ cyclic nucleotide 3′ phosphodiesterase and its mRNA in the rat nervous system. *J. Neurochem.* 51:859–868.

Trapp, B.D., S.B. Andrews, C. Cootauco, and R.H. Quarles. 1989. The myelin-associated glycoprotein is enriched in multivesicular bodies and periaxonal membranes of actively myelinating oligodendrocytes. *J. Cell Biol.* 109:2417–2426.

Trapp, B.D., G.J. Kidd, P.E. Hauer, E. Mulrenin, C. Haney, and S.B. Andrews. 1995. Polarization of myelinating Schwann cell surface membranes: role of microtubules and the trans-Golgi network. *J. Neurosci.* 15:1797–1807.

Warner, L.E., M.J. Hilz, S.H. Appel, J.M. Killian, E.H. Kolodny, G. Karpati, S. Carpenter, G.V. Watters, C. Wheeler, D. Witt, et al. 1996. Clinical phenotypes of different *MPZ* (P_0) mutations may include Charcot-Marie-Tooth type 1B, Dejerine-Sottas, and congenital hypomyelination. *Neuron.* 17:451–460.

Weimbs, T., S.H. Low, S.J. Chapin, and K.E. Mostov. 1997. Apical targeting in polarized epithelial cells: there's more afloat than rafts. *Trends Cell Biol.* 7:393–399.

Weinberg, H.J., and P.S. Spencer. 1976. Studies on the control of myelinogenesis. II. Evidence for neuronal regulation of myelin production. *Brain Res.* 113:363–378.

Windebank, A.J., P. Word, R.P. Bunge, and P.J. Dyck. 1985. Myelination determines the caliber of dorsal root ganglion neurons in culture. *J. Neurosci.* 6:1563–1567.

Wrabetz, L., M.L. Feltri, A. Quattrini, D. Imperiale, S. Previtali, M. D'Antonio, R. Martini, X. Yin, B.D. Trapp, L. Xhou, et al. 2000. P_0 overexpression causes congenital hypomyelination of peripheral nerves. *J. Cell Biol.* 148: 1021–1033.

Yin, X., J. Peterson, M. Gravel, P.E. Braun, and B.D. Trapp. 1997. CNP overexpression induces aberrant oligodendrocyte membranes and inhibits MBP accumulation and myelin compaction. *J. Neurosci. Res.* 50:238–247.

Yin, X., T.O. Crawford, J.W. Griffin, P.-H. Tu, V.M.Y. Lee, C. Li, J. Roder, and B.D. Trapp. 1998. Myelin-associated glycoprotein is a myelin signal that modulates the caliber of myelinated axons. *J. Neurosci.* 18:1953–1962.